Progress In Electromagnetics Research C, Vol. 129, 17–34, 2023

Low SAR Dual-Band Circularly Polarized Wearable RFID Antenna Using FSS Reflector with Reduced EMI

Shivani Sharma[1, *], Malay R. Tripathy[1], and Ajay K. Sharma[2]

Abstract—A circularly polarized dual band wearable antenna using a frequency selective surface backed reflector for radio frequency identification reader resonating at global ultra-high frequency band (860–960 MHz) and ISM band (2.4 GHz) is proposed in this work. For circular polarization, the corner is truncated at the opposite end of a square patch with periodic slots over the patch for getting an orthogonal electric field in both the X and Y axis directions. Another truncated inner square slot patch miniaturizes the antenna further for stable frequency response. Finally, the periodic frequency selective surface-based reflector is used for gain enhancement and crosstalk reduction. The simulated and measured results for antenna over human body are plotted against the required bandwidth. The return loss and maximum radiated gains of −31 dB and 8.30 dB are achieved at a resonating frequency of 2.4 GHz with the reading range and Specific Absorption Rate (SAR) of 6.98 m and 0.77 watt/kg, respectively. At 865 MHz, the return loss and maximum radiated gain are −23 dB and 5.31 dB with the reading range and SAR of 5.21 m and 0.65 watt/kg, respectively. The proposed Ultra-High Frequency (UHF) RFID antenna is circularly polarized with the axial ratio bandwidth less than 3 dB with approximately 15% (860–965 MHz and 2.4–2.45 GHz) range. The designed wearable antenna provides better isolation when FSS is incorporated while enhancing the gain for longer read range. The FSS reflector below the antenna reduces the SAR for on-body wearable applications. This RFID antenna can be used efficiently for WBAN applications as a portable RFID reader wearable antenna for remote sensing and real time monitoring.

1. INTRODUCTION

The Radio Frequency Identification (RFID) technology in recent years is being effectively utilized in Wireless Body Area Network (WBAN) for various wireless real time monitoring applications [1–3]. Generally, RFID antenna resonates at low frequency (125–134 kHz), high frequency (13.56 MHz), global ultra-high frequency (860–960 MHz), and microwave range at ISM 2 and 5 GHz bands. The RFID system always consists of a functioning RFID tag, commonly known as a transponder and an RFID reader, commonly known as an Interrogator. The operating principle of any RFID system is concentrated on the transmission of electromagnetic (EM) waves from the RFID reader received by the tag. Then again, the data collected by the RFID tag is transmitted back to the RFID reader in the form of EM waves. The data interpreter or the middleware is generally developed within the RFID reader but can be connected externally if required. RFID system is further categorized according to the required range of frequency as per international standards. The RFID standards can be classified based on Industry specified standards to regulate the RFID operation in industries or National regulations set by specific country to regulate its local RFID system or Regional standards to regulate the RFID system within that particular region or Global standard set by international bodies for regulating the RFID

Received 20 October 2022, Accepted 3 January 2023, Scheduled 22 January 2023
* Corresponding author: Shivani Sharma (shivaniaeri25@gmail.com).
[1] Department of Electronics and Communication Engineering, Amity University, Noida 201313, Uttar Pradesh, India. [2] Antenna Development and Engineering Department in Bharat Electronics Ltd., Ghaziabad 201010, Uttar Pradesh, India.

operations over the entire world. Global organizations that define international standards include the International Standards Organization (ISO), the International Electrotechnical Commission (IEC), EPC global (GS1), and the Joint Technical Committee (JTC1). A few regional organizations such as Federal Communication Commission (FCC), the European Telecommunications Standards Institute (ETSI), and Spectrum Compliance Asia also regulate the RFID standards [4].

Therefore, the focus area of most of the researchers is to effectively extract the original data from reader via tag. To accurately achieve this, a hindrance free communication link between the reader and the tag is required so that the transmitted data is as accurate as possible when being received. Hence, effective measures and optimization techniques can be implemented in RFID antenna, since RFID antenna is the ultimate component in the RFID system which creates the transmission link between the reader and the tag. If the RFID reader is known as the brains of the RFID system, then RFID antennas are considered as the arms of the RFID system since they are responsible for transmitting and receiving the Radio Frequency (RF) waves to and from the tags through the reader [5]. The global Ultra-High Frequency (UHF) band is regulated by GS1 standards for their effective operations. Most of the cases requires the use of passive UHF antenna for RFID applications in WBAN, since the high frequency of active tags and battery weight can cause unwanted adverse effects on human body [6, 7]. Also, for the mass deployment of RFID system in WBAN and cost effectiveness, a passive UHF RFID system is preferred for WBAN applications. The design obligations for the wearable antenna by Federal Communication Commission (FCC) is distinctive compared to traditional antennas for Body Centric Communication (BCC) [8]. The work on reconfigurability structure is recently explored by various researchers [9–15], which uses low-capacitance, low-power consumption diodes to digitally control the modification of the radiation pattern making it reconfigurable, but due to active components the antenna structure may not be practically effective when being used in WBAN. Similar to this work, Haydhah et al. [16] presented a reconfigurable antenna using P-I-N diode with two modes to switch with the total radiated gain of 1.6 dB. Numerous issues can be raised due to on-body RF coupling effecting the performance of wearable devices [17]. The EM radiation has a damaging impact on the human tissues; therefore, radiation level must adhere to the Specific Absorption Rate (SAR) level [18]. The resonance frequency of the designed antenna also gets affected by the human on-body losses. After considering all the challenges that can affect the wearable antenna performance in a complex environment, the wearable substrate material must be carefully chosen [19, 20]. The substrate material used for wearable antennas must be high heat resistant, highly absorptive, and flexible. The physical constraints include some other requirements such as low SAR level, miniaturized structure, compactness, flexibility, low power dissipation, high bending capabilities, low loss tangent, and low dielectric value [21, 22]. The RFID communication link operates for unique frequencies, and accordingly, the SAR and Effective Isotropic Radiated Power (EIRP) standards/limits are standardized by several countries.

The RFID system implication in WBAN is a critical area of research for wireless sensing network, and advancements in the technology can lead to a variety of future applications. This work is based on the design, simulation, fabrication, and testing of the passive Circularly Polarized (CP) dual-band wearable antenna using frequency selective surface (FSS) reflector for portable RFID reader which can be used for global RFID range (860–960 MHz) and 2.4 GHz with enhanced gain and augmented read range. The CP reader antenna is essential for better omnidirectional scanning of the tags without the alignment of the reader at any particular angle [23, 24]. The CP RFID antenna has reduced multipath effect, which can avoid misread of data transmitted or complete loss of the transmitted data due to path loss since it is transmitting in all planes [25]. It is achieved by a traditional truncating method of square patch, but in this design, the periodic slotting on the patch is also done for maintaining the polarization throughout. Further, the FSS is used as a reflector to enhance the gain and directivity of the proposed RFID antenna without changing the structure itself. This antenna structure is fabricated on a wearable material for making it a portable reader antenna for WBAN healthcare applications [refer Figure 1]. This work is focused on the enhancement of gain and directivity of the portable RFID reader with directional transmission with reduced EMI using FSS as a reflector.

The use of FSS here in RFID system overcomes the major challenges faced by the RFID system in WBAN [26–29]. Also, miniaturizing the antenna slotting is done in ground as well as on the conducting patch. The FSS-backed ground offers gain enhancement, frequency filtering, better directivity, reduced Electro-Magnetic Interference (EMI), and better-read range for passive RFID reader. The use of a low-

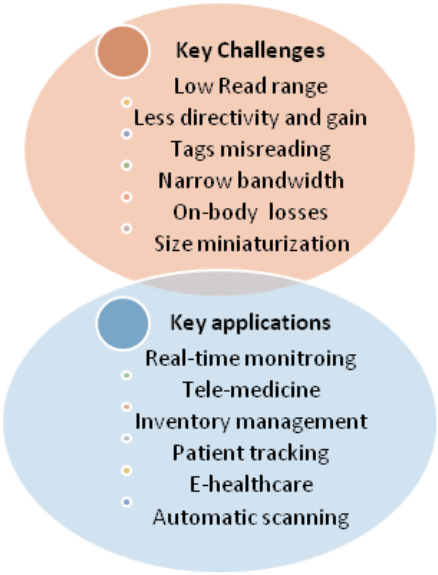

Figure 1. Key challenges and applications of UHF RFID system in WBAN for real-time wireless communication.

loss flexible substrate material for fabrication makes it efficient to be easily implemented for wearable portable WBAN applications. This paper is organized as follows. Section 1 discusses the importance of the research area in the form of literature review. Section 2 discusses the designing and geometrical modelling of the proposed antenna structure. Section 3 is focused on analytical modelling of the proposed antenna. Section 4 discusses the simulated results along with the validation of experimental results. Section 5 gives the conclusion and future implications of the presented research work.

2. DESIGN METHODOLOGY OF PROPOSED UHF RFID ANTENNA

In the proposed antenna design, a low dielectric constant polymer-based flexible substrate material Teflon/Polytetrafluoroethylene (PTFE) with 0.5 mm of thickness is used for the fabrication with dimension S_x and S_y. The designed antenna resonates at UHF global band (860–960 MHz) for WBAN applications resonating at 865 MHz. The permittivity (ε_r) is 2.2, and loss tangent ($\tan\delta$) value is 0.002 which is required for low frequency wearable applications. The iteration procedure of the conducting copper patch is given in Figure 2. The methodological steps for the antenna's evolution process are

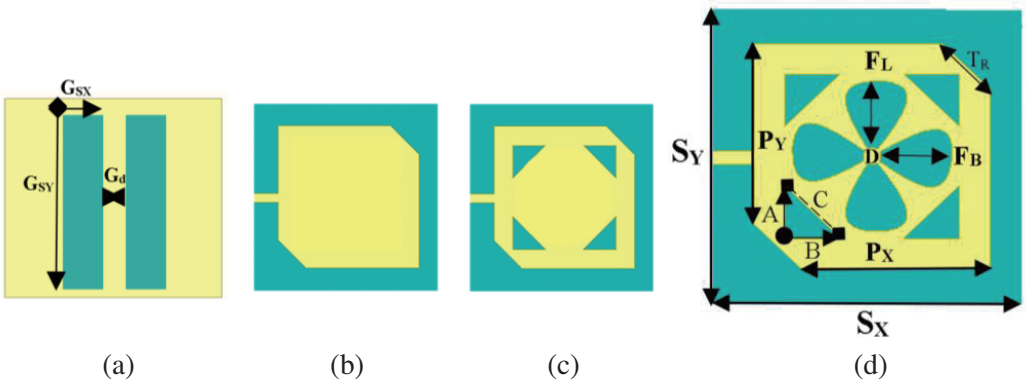

Figure 2. (a) Defective Ground structure. (b) Iteration 1. (c) Iteration 2. (d) Iteration 3 with Final antenna geometry with geometrical description.

given below with the advantages, and each stage offers:

Step 1(Iteration 1): Initially, the square patch is etched over the substrate as a radiating element [Figure 2(b)]. The dimension of conducting patch is specified as P_x (width) and P_y (length) given in Table 1. To achieve circular polarization, the truncated corner slotting is employed with slant height (c) of 21.2 mm and equal sides of 15.5 mm. This is the simplest technique out of available techniques, which gives unform electric field orthogonal to both the X axis and Y axis.

Step 2(Iteration 2): Then, smaller triangular slots at each corner of the square patch are introduced inside the patch [refer Figure 2(c)]. The dimension of inner triangular patch is mentioned in Table 1 as side (A), another side (B), and slant height (C).

Step 3(Iteration 3): Now, the flower-shaped slot with radius R is etched over the truncated loop patch which improves the uniformity of generated current over the patch at every point [Figure 2(d)]. All the petals of the flower-shaped design are equal with length and width denoted as F_L and F_B [refer Table 1]. The finalized geometry of the proposed RFID antenna is given in Figure 2(d) with ground plane dimension of G_x and G_y. The lowest resonant frequency for dominant mode (1, 0) for square patch is used to find geometrical parameters of antenna where L is the length of the antenna, c the speed of light, and ε_{reff} the effective dielectric constant using following equations [30].

$$f_{1,0} = \frac{c}{2L\sqrt{\varepsilon_{reff}}} \tag{1}$$

$$(\text{If } (w/h) < 1) \quad \varepsilon_{reff} = \frac{\varepsilon r + 1}{2} + \frac{\varepsilon r - 1}{2}\left[\frac{1}{\sqrt{1 + 12\left(\frac{h}{w}\right)}} + 0.04\left(1 - \left(\frac{w}{h}\right)\right)^2\right] \tag{2}$$

$$(\text{If } (w/h) > 1) \quad \varepsilon_{reff} = \frac{\varepsilon r + 1}{2} + \frac{\varepsilon r - 1}{2}\left[\frac{1}{2\sqrt{1 + 12\left(\frac{h}{w}\right)}}\right] \tag{3}$$

where w is the width of the patch, also denoted as P_Y; L is the length of the patch, also denoted as P_X; and h is the height/thickness of the substrate, also denoted as t.

The iterative process of different stages of patch structures are processed and analyzed in terms of reflection coefficient v/s frequency response for required bandwidth (refer Figure 3). The microstrip feed of $\lambda/2$ is given to excite the antenna with the dimensional length 4.7 mm and 13 mm using lumped port excitation. Defective Ground Structure (DGS) is used for dual band transmission using two rectangular slots G_{sx} and G_{sy} with dimension 10 mm by 60 mm in X and Y directions, respectively. The values of geometric parameters of designed antenna are calculated using the microstrip transmission line theory and Babinet's principle which are presented in Table 1.

Table 1. Geometrical description: proposed flexible passive UHF RFID antenna.

Parameters	Measured value (mm)
P_X, P_Y	$65 * 65$
A, B, C	$17.5 * 17.5 * 24.7$
T_R	21.2
F_L, F_B	$22.8 * 19.5$
S_D	5
G_{Sx}, G_{Sy}, G_d	$10 * 60 * 5$
$S_X(G_X)$, $S_X(G_Y)$	$100 * 100$
D	5.5

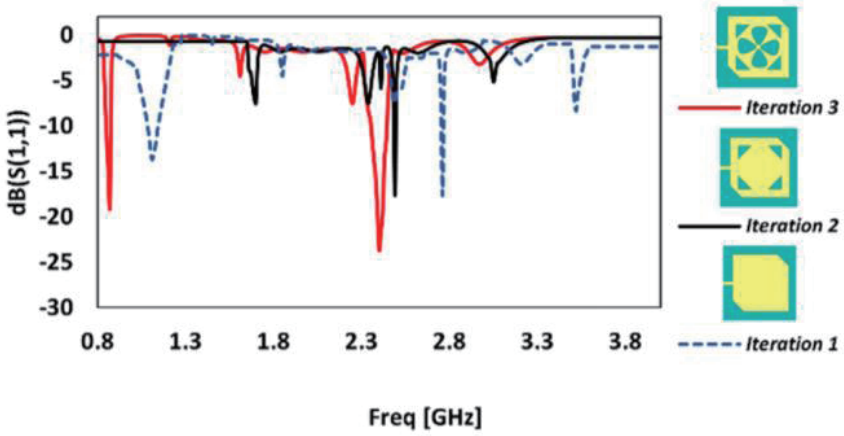

Figure 3. Reflection coefficient of all the iterative structures.

2.1. Proposed Novel Frequency Selective Surface's Configuration

Lastly, the novel frequency selective surface-backed reflector having periodic slots is placed which improves the overall directivity and gain of the proposed antenna. It also helps to reduce the EMI due to the presence of multiple tags. The basic principle for FSS spectral domain analysis can be explained using Floquet's port principle which states that when an incident wave illuminates an infinite, periodic, planar sheet, each unit cell on an array of periodic structure must generate equal current and electric field. The in-band waves are transmitted in phase with that of incident wave, and out-band waves are reflected back using the FSS reflector as ground plane and can be seen in Figure 4 where λ is the highest resonating frequency, i.e., 2.4 GHz.

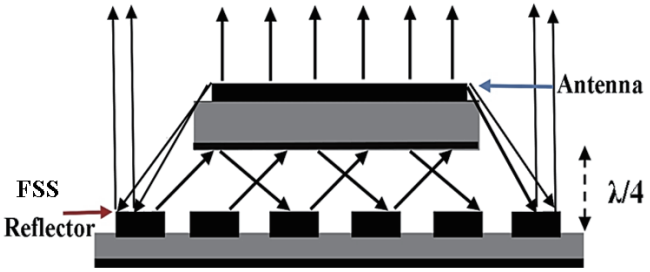

Figure 4. Proposed RFID antenna arrangement with FSS reflector.

The geometrical parameters of FSS unit cells are calculated using the theory of Floquet's port [31]. The unit cell of the proposed novel FSS periodic structure with 8 by 8 array with dimensions 150 mm by 150 mm having D equal to 3.6 mm is finally etched over the wearable substrate to get desired stable frequency response [refer Figure 5(a)]. The proposed RFID antenna arrangement with FSS backed ground sheet as a reflector is shown in Figures 5(b) and (c). The substrate is sandwiched between the reflective FSS array patch and the conductive patch. The dimension of proposed FSS sheet and unit cell is given in Table 2 with all the calculated parameters.

The important parameters for designing the novel FSS unit cell are overall array length, unit cell length, and inter-spacing element which can be calculated using given equations [31]:

$$\text{Overall array length } (a) \approx \lambda_L/3 \tag{4}$$

$$\text{Length of the unit cell } (S_L);\ \frac{\lambda_L}{25} \leq S_L \leq \frac{\lambda_L}{15} \tag{5}$$

$$\text{Inter-element spacing } (D) \leq 0.5\lambda_L \tag{6}$$

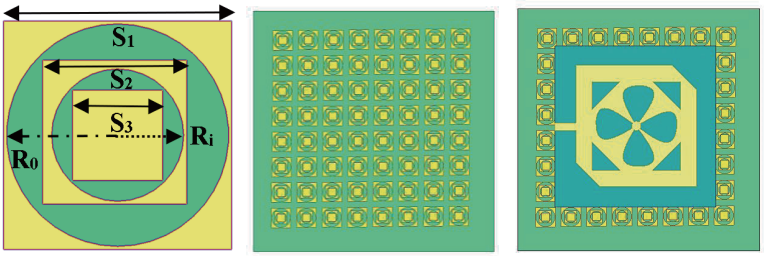

Figure 5. (a) Unit cell of proposed flexible FSS reflector sheet. (b) 8 by 8 array of FSS reflector. (c) Proposed flexible RFID antenna with FSS reflector.

Table 2. Geometrical description: proposed flexible FSS sheet and unit cell.

Parameters	Measured value (mm)
S_1	12.1
S_2	7.7
S_3	4.8
R_i	3.5
R_o	5.9

On-set grating condition depends on the incident wave angle which if occurring can lead to out of phase transmission of higher order Floquet's waves in space. Considering guided wavelength of overall FSS array, the inter-element spacing (D) is given below [31]:

$$D = \frac{\lambda g \times n}{(\sin\eta + \sin\eta g)}; \quad \text{Where} \quad \lambda g = \frac{c}{fg} \tag{7}$$

λ_g is the guided wavelength, c the speed of light, and n the number of elements. Considering the case where the incident wave is perpendicular, i.e., $\eta_g = 90°$, the inter-element spacing becomes:

$$D = \frac{\lambda g \times n}{(\sin\eta + 1)} \tag{8}$$

To study the reflector behavior of FSS-sheet, two major parameters need to be studied, i.e., effective permeability (μ) and permittivity (ε) are derived from reflection coefficient against the resonant frequency. The reflection coefficient and transmission coefficient can be plotted for incident waves at 90° to study magnetic and electrical properties of FSS sheet. Using Thevenin's circuit modelling along with time dependence of $j\omega t$, the magnetic susceptibility (χ_m) and electrical susceptibility (χ_e) for a lossless loop or dipole can be calculated. The value of relative negative permittivity and permeability at resonant frequencies can be calculated in terms of susceptibility as follows:

$$\varepsilon_r = \frac{\varepsilon}{\varepsilon_o} = 1 + \chi_e \tag{9}$$

$$\mu_r = \frac{\mu}{\mu_o} = 1 + \chi_m \tag{10}$$

Therefore, it can be concluded that the frequency selective surface has reflective behavior only when its permittivity becomes negative at reflection frequencies [32]. The effective permittivity and permeability in terms of S parameters are plotted against the resonant frequencies and given below in Figure 6 and Figure 7.

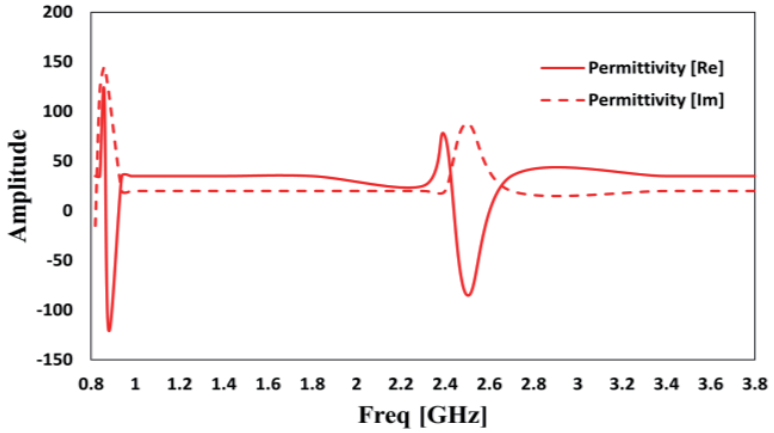

Figure 6. Real and imaginary part of permittivity (ε).

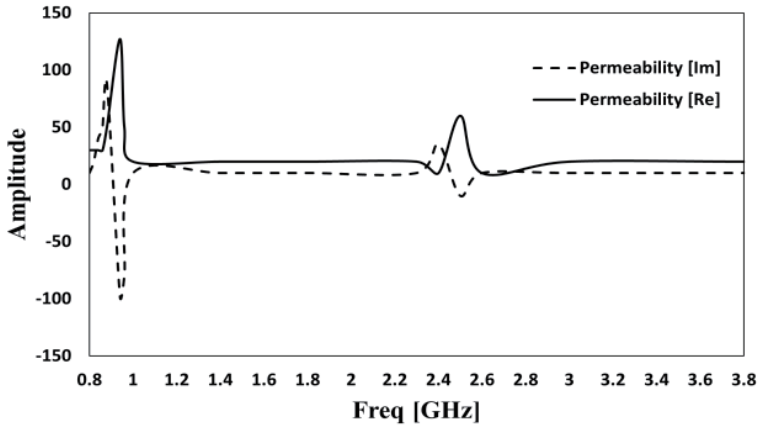

Figure 7. Real and imaginary part of permeability (μ).

3. ANALYTICAL MODELLING OF THE PROPOSED RFID ANTENNA

In this section, the performance of the proposed wearable RFID antenna is analyzed and examined on the basis of various characteristic properties by means of Equivalent Circuit Modelling (ECM), Specific Absorption Rate (SAR) analysis, bending analysis and power analysis.

3.1. Equivalent Circuit Modelling of Proposed Antenna

The topology of overall equivalent circuit model of the proposed wearable UHF RFID antenna resonance model is shown in Figure 8, where Z_{ps} is the total impedance due to four triangular slots on the patch, Z_{FL} the impedance due to center flowered slot, Z_P the overall impedance of the microstrip patch, and Z_F the impedance of the microstrip feed line. At lower frequencies, capacitance dominates the overall effect on the input impedance of the antenna, and at higher frequencies, inductance dominates. The equivalent impedances for both the cases are given below:

$$Z_{eq}(f_L) = \frac{1}{2\pi f C_{0,0}} \tag{11}$$

$$Z_{eq}(f_H) = 2\pi f C_{\infty} \tag{12}$$

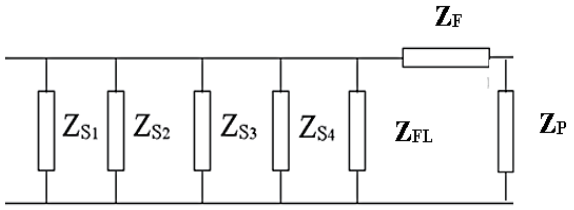

Figure 8. Resonance circuit for proposed antenna.

where $C_{0,0}$ is the overall capacitance at lower frequencies, and L is the overall inductance at higher frequencies. The overall resonance network is represented by adding the RLC model of FSS reflector in parallel with that of antenna with feedline. The impedance of the antenna patch is given by:

$$Z_p = \frac{1}{\frac{1}{j\omega L} + j\omega C + \frac{1}{R}} \tag{13}$$

$$Z_{ps} = \frac{1}{Zp} + \frac{1}{Zs_1} + \frac{1}{Zs_2} + \frac{1}{Zs_3} + \frac{1}{Zs_4} \tag{14}$$

$$Z_{ant} = \frac{1}{Zp} + Z_{FL} + Z_{ps} + Z_F \tag{15}$$

Further, the resonance model of proposed antenna is represented based on R,LC network in Figure 9 where L_1, L_2, L_3, L_4 and C_1, C_2, C_3, C_4 are the inductors and capacitors of slotted triangles respectively in series. The center flowered slot or petals are represented by L_{F1}, L_{F2}, L_{F3}, L_{F4} and C_{F1}, C_{F2}, C_{F3}, C_{F4} in parallel resonance which are in parallel with the capacitor of center bud slot C_c. The square microstrip patch has resonance, i.e., L_p, R_P, and C_P, which is in shunt with the series resonance of microstrip feedline with L_M, R_M, C_M as inductor, resistor, and capacitor, respectively.

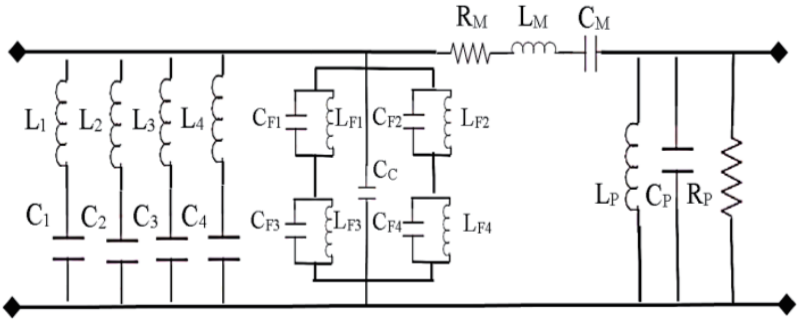

Figure 9. ECM of proposed UHF RFID antenna.

The ECM for the proposed RFID antenna with FSS reflector is based on the transmission line theory using parallel resonance condition by calculating S_{11} parameter and is given in Figure 10. Overall inductance and capacitance can be modified by modifying gap between the unit cells' inter-element spacing (D), overall length of the array (a), and thickness (t) of the metallic layer. The overall inductance of unit cell and FSS array is given in following equations:

$$Cg \approx \varepsilon_r \varepsilon_o \frac{(a \times t)}{D} \tag{16}$$

where $\varepsilon_o = 8.85 \times 10^{-12}$ f/m, t = thickness of the metallic patch, and a is the overall length of the FSS reflector array

$$Cs \approx \varepsilon_r \varepsilon_o \times t \tag{17}$$

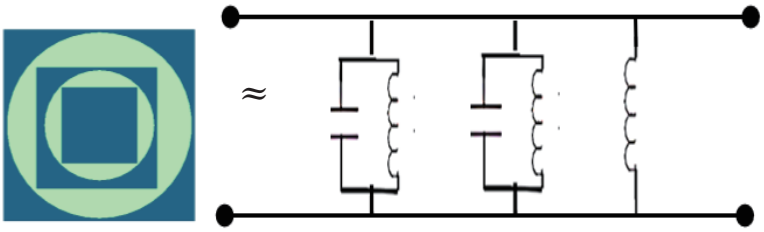

Figure 10. ECM of proposed UHF RFID antenna unit cell ($Ls =$, $L_T = Cs = C_T$).

Therefore, the total C_T can be calculated using given equation:

$$C_T \approx \varepsilon_r \varepsilon_o \times t \frac{(a+D)}{D} \tag{18}$$

Now, the series inductance of unit cell and total array inductance is given by:

$$Ls \approx 2a \left[\log \frac{2a}{t} + \frac{1}{2}\right] \tag{19}$$

$$L_T = \frac{L_S}{6} \quad \text{Therefore,} \quad L_T = \frac{a}{3}\left[\log \frac{2a}{t} + \frac{1}{2}\right] \tag{20}$$

3.2. Floquet's Port Analysis

The analysis of proposed FSS reflector is performed using Floquet's port analysis, and the reflection coefficient is plotted against the required range of frequencies in Figure 11. The port excitation is given on the top and bottom faces of the waveguide. For unit cell analysis as an infinite plane the length of the waveguide should be greater than $\lambda/4$, and 2 pairs of master slave boundaries are given on each side face of the Floquet's port to eliminate higher order modes.

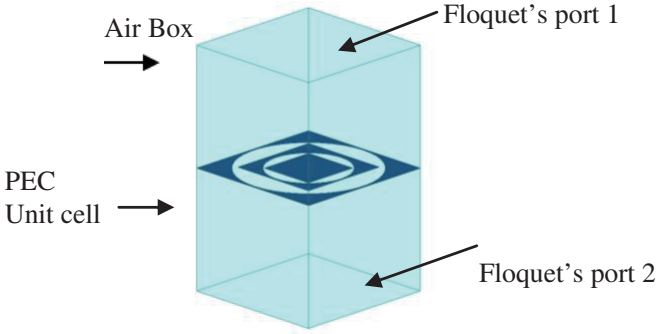

Figure 11. Floquet's port analysis of proposed FSS unit cell.

The transmission and reflection coefficient for proposed FSS unit cell is given in Figure 12 showing the transmitting response for required resonating frequency and reflecting response for unrequired frequency range in UHF band.

The final optimum distance between the FSS reflector and the proposed antenna is analyzed and shown in Figure 13. It is noticeable that the return loss is better at 2.4 GHz when FSS reflector is placed at a distance of 30 mm keeping the $\lambda/4$ distance at highest resonating frequency from radiating antenna maintained using a foam spacer.

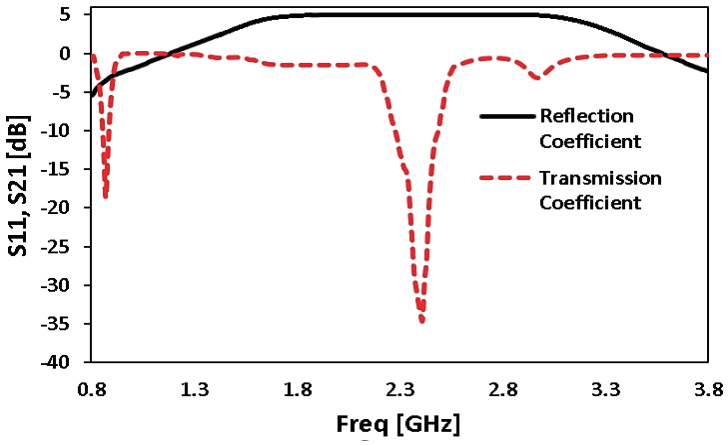

Figure 12. Transmission (S_{11}) and Reflection coefficient (S_{21}) of FSS unit cell.

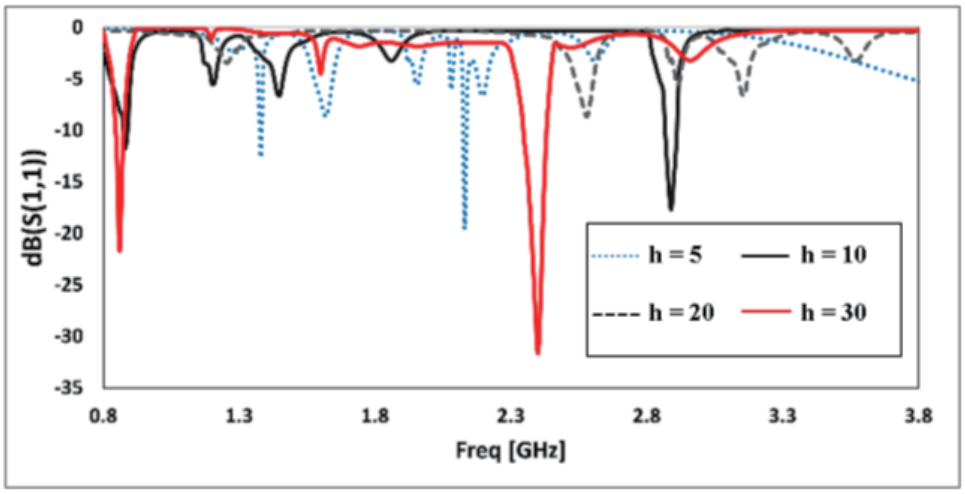

Figure 13. Plot for optimum distance between the antenna and FSS reflector.

3.3. SAR Analysis

The designed wearable antenna can be detuned owing to the absorption of large amount of radiated power by human body, and thus gain of the antenna is mostly reduced. The value of constant (ε_r), conductivity (σ), mass density (D), and thickness (t) must be considered before designing the antenna for wireless wearable communication in WBAN shown in Figure 14 in which all four layers, i.e., skin, fat, muscle, and bone are represented with different characteristics.

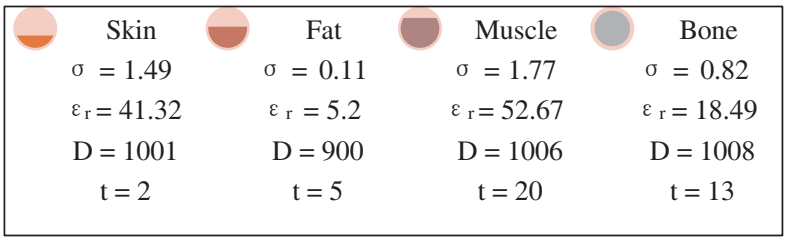

Figure 14. Human tissue layer's properties for SAR analysis.

To keep the antenna within the safer limit, the Federal Communication Commission (FCC) has set some specific SAR value of ≤ 1.6 Watt/kg over 1 g of tissue which is usually measured over 1 gram or 10 grams of tissue weight and is given in the following equation [33]:

$$\text{SAR} = \frac{\sigma}{\rho} E_{rms}^2 = \frac{1}{V} \int \frac{\sigma(r) |E(r)|^2}{\rho(r)} dr \tag{21}$$

where V is the volume of the sample, E the mean RMS value of the electric field (V/m), σ the conductivity (S/m), and ρ the density of the tissue (kg/m^3). The IEEE's standard for SAR is equivalent to 2 watts/kg over 10 g of tissue according to section C95.1-2005 [33]. This value is also recognized by the International Commission on Non-Ionizing Radiation Protection (ICNIRP). The amount of EM radiations absorbed may lead to a change in temperature of tissue and is given by:

$$\text{SAR}(\Delta T) = C(\Delta T) \tag{22}$$

where (ΔT) is the duration of exposure, and C is the discharged heat. To validate the effect of FSS reflector sheet the SAR values are plotted for both the cases, i.e., one with antenna only and the other with FSS reflector in Figures 15(a) and (b).

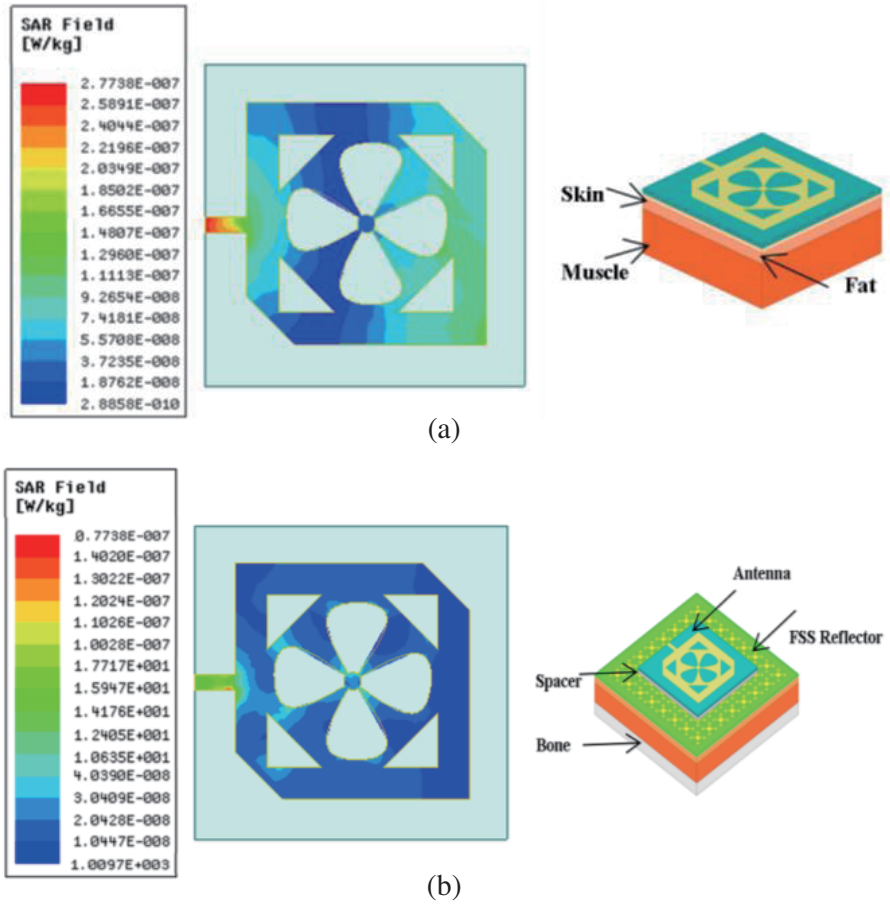

Figure 15. SAR value evaluation for 1 gm of human tissue at 2.4 GHz. (a) Antenna. (b) Antenna with FSS reflector.

It can be seen that the SAR field is within the safety limit, and surface charge is also negligible. In comparison, it is clearly evident that FSS as a reflector reduces the average SAR value. Also, FSS reflector helps the antenna to maintain the stable response for required range while reflecting back the harmful surface wave from the body in the direction of transmission.

4. SIMULATED AND EXPERIMENTAL RESULTS OF PROPOSED FSS BACKED ANTENNA STRUCTURE

4.1. Return Loss for Impedance Matching

For matching the input impedance characteristics of the antenna, the reflection coefficient S_{11} (dB) is plotted against resonant frequencies in Figure 16.

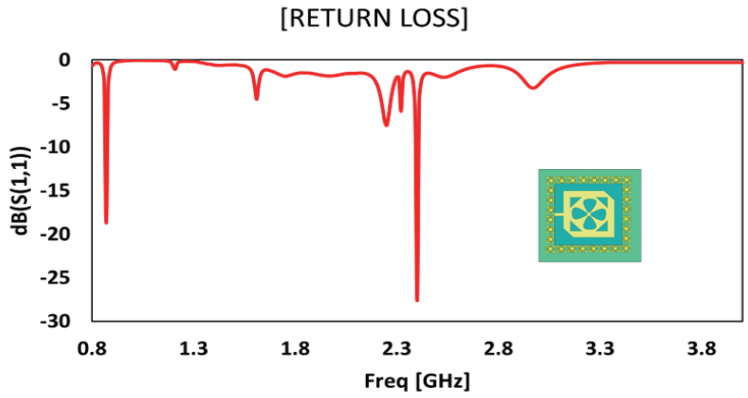

Figure 16. Reflection coefficient of UHF RFID antenna with FSS reflector.

4.2. Radiated Gain and Pattern

The measured value of gain at lowest frequency as well as higher frequency is incremented using FSS reflector. The back radiation is also reduced due to FSS reflector. The 3D radiation graph against frequency is plotted and is shown in Figure 17. The radiation patterns at different values of φ, i.e., 0°, 90°, 180°, 360°, keeping θ constant are shown in Figure 18.

4.3. Current Distribution

The electric field and magnetic field are shown in Figure 19 given below with constant electric and magnetic fields obtained to maintain the uniform surface current on the antenna's patch.

However, the electric field has a higher value in V/m than the magnetic field A/m in both cases because of the patch type radiating element. It is evident in given figure that E and H fields are equally distributed from center slot to the edges.

4.4. Axial Ratio

The axial ratio (AR) is an essential factor to be considered while any circularly polarized antenna is designed, and it must be lower than 3 dB (refer Figure 20). The AR is the ratio of the major axis (largest axis) to the minor (the smaller axis), and it is given in the following equation [34].

$$\mathrm{AR} = \left|\frac{Ex}{Ey}\right| \leq 1 \tag{23}$$

where E_x and E_y are two orthogonal complex values of field components in the X direction and Y direction. If one of the components out of them is zero, the polarized field becomes linear. If none of them is zero, we can compute the circularly polarized field. If AR is perfectly equal to 1, the antenna is circularly polarized or else tilted, and the tilt angle for elliptical polarization is calculated using the given equation:

$$\frac{\angle Ex}{\angle Ey} = 2\tau \tag{24}$$

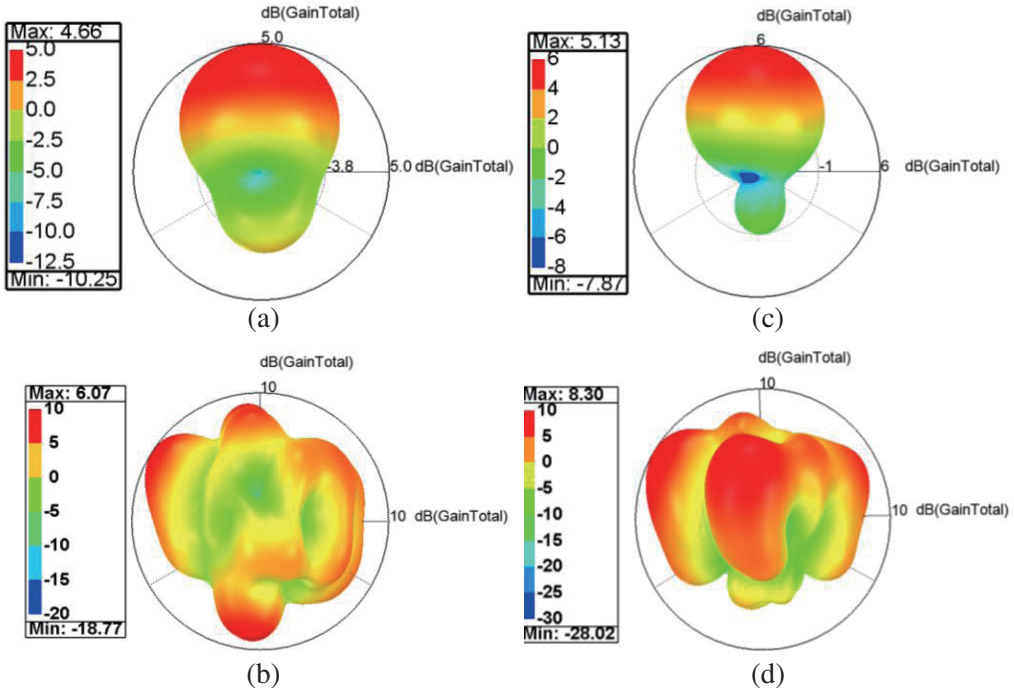

Figure 17. 3D gain plot. (a) Proposed antenna at 865 MHz. (b) Proposed antenna at 2.4 GHz. (c) Proposed antenna with FSS Reflector at 865 MHz. (d) Proposed antenna with FSS Reflector at 2.4 GHz.

where τ is the tilt angle and $E_x = E_x \cos\tau - E_y \sin\tau$; $E_y = E_x \sin\tau + E_y \cos\tau$.

The proposed antenna structure is fabricated, and the experimental results are measured using Vector Network Analyzer (VNA). The fabricated FSS & antenna are given in Figures 21(a), (b), (c). The fabricated antenna is placed above the FSS reflector sheet using foam spacer for the final proposed structure, and parameters are given in Table 3.

Table 3. Result of proposed RFID antenna.

	Frequency	**Return Loss (dB)**	**Max. Gain (dB)**	**Read range**	**Max. SAR (watts/kg) for 10 gm of tissue**
ANTENNA	865 MHz	−19	4.66	2.49	2.43
ANTENNA	2.4 GHz	−27	6.07	3.97	2.77
ANTENNA+ FSS REFLECTOR	865 MHz	−23	5.31	5.21	0.65
ANTENNA + FSS REFLECTOR	2.4 GHz	−31	8.30	6.98	0.77

The simulated results are validated by experimental results which shows a good agreement between simulated and measured values (refer Figure 22). The fabricated antenna is tested, and measured results are later compared with simulated result for better analysis. The measured read range is 6.52 m with the measured gain of 7.98 dB. The presented work is justified in Table 4, which comprises a brief comparison between this research work and available research work in same applicable field.

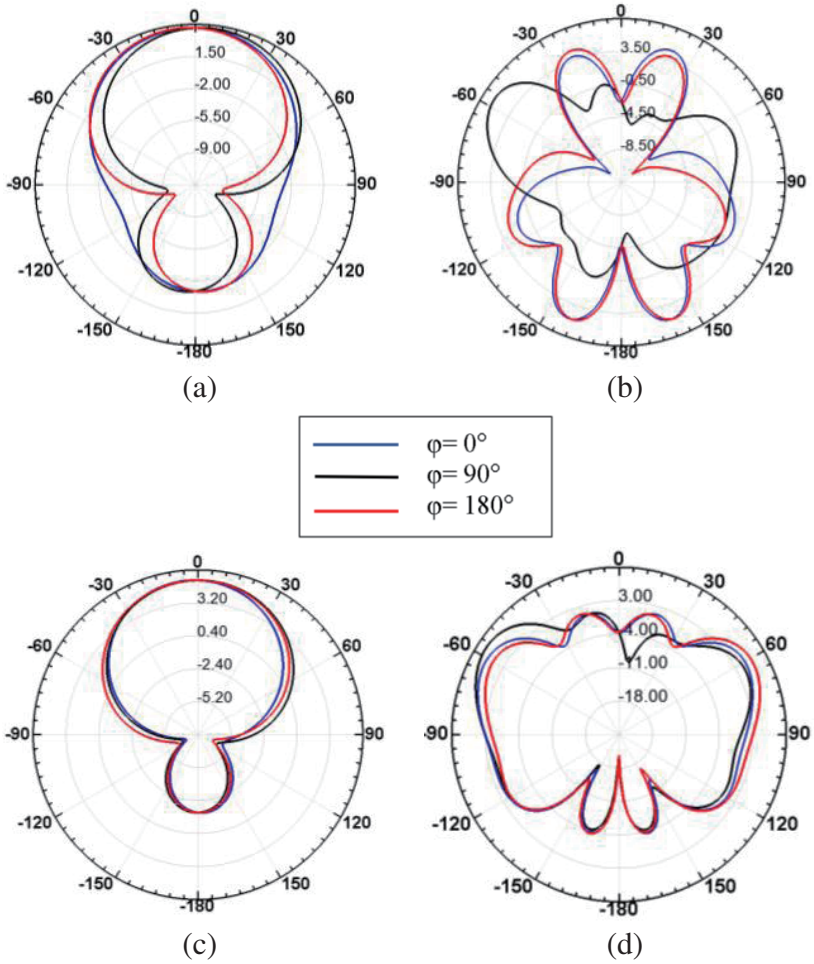

Figure 18. Radiation pattern for $\varphi = 0°$, 90° and 180° with constant θ, (a) proposed antenna at 865 MHz, (b) proposed antenna at 2.4 GHz, (c) proposed antenna with FSS reflector at 865 MHz, (d) proposed antenna with FSS reflector at 2.4 GHz.

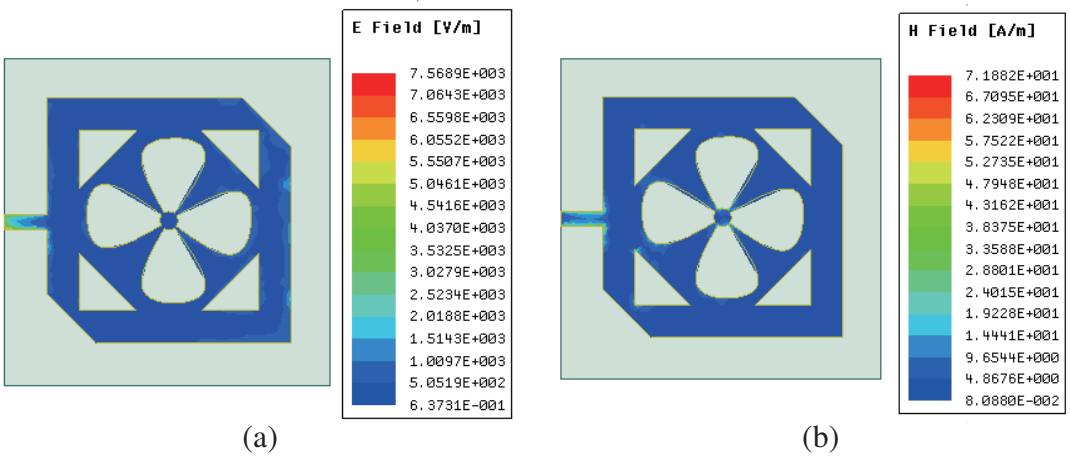

Figure 19. (a) Electric field distribution. (b) Magnetic field distribution at 2.4 GHz.

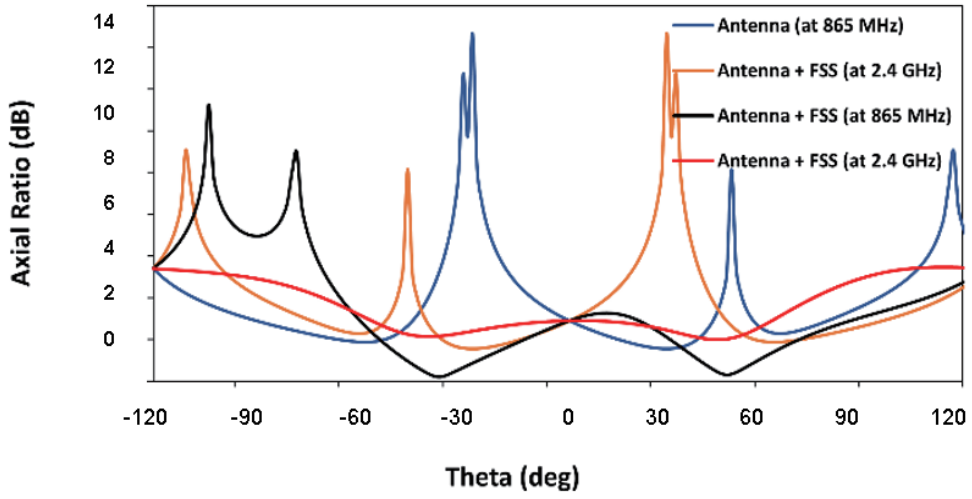

Figure 20. Axial ratio (AR) for all theta vales at $\theta = 0°$ and $\varphi = 0°$ at $\theta = 90°$ and $\varphi = 90°$.

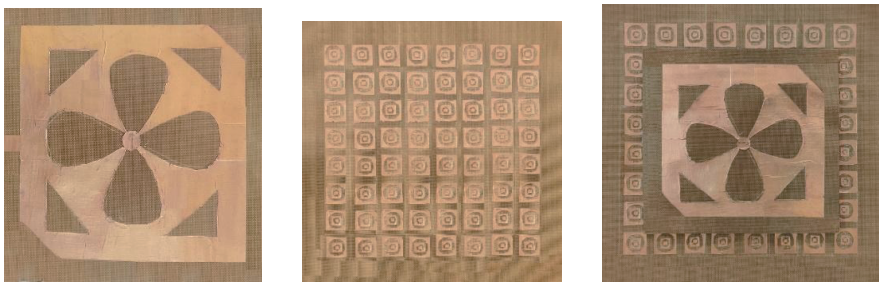

(a) (b) (c)

Figure 21. (a) Fabricated antenna. (b) Fabricated FSS reflector. (c) Fabricated antenna with FSS reflector.

Table 4. Comparison of previous work with this proposed research work.

Ref. No.	Substrate	Frequency	Dimension	Return Loss (dB)	Max. Gain (dB)	Read range (m)	3 dB Axial Ratio (%)	Max. SAR (watts/kg)
[35]	FR4	915 MHz, 2.45 GHz	210210 30	−23	6.25	N.A.	5.25	N.A.
[36]	Jeans	2.4 GHz	$60 * 60 * 2.4$	−45	6.55	N.A.	8.3	0.05
[37]	Polyimide	2.4 and 5.8 GHz	$72 * 72 * 5$	−25	−4.1	N.A.	9.2	0.7
[38]	FR4	915, 2.4	$85 * 85 * 1.6$	−30	2.2	1.53	10	N.A.
[39]	Conductive yarn	866 MHz	$71 * 65$	−20	−2.6	4.6	5	3.6
[40]	EPDM	915 MHz	$243 * 263 * 4$	−25	−5.5	2	N.A.	0.9
This work	Teflon	865 MHz, 2.4 GHz	$150 * 150 * 10$	−31	8.30	7	15	0.77

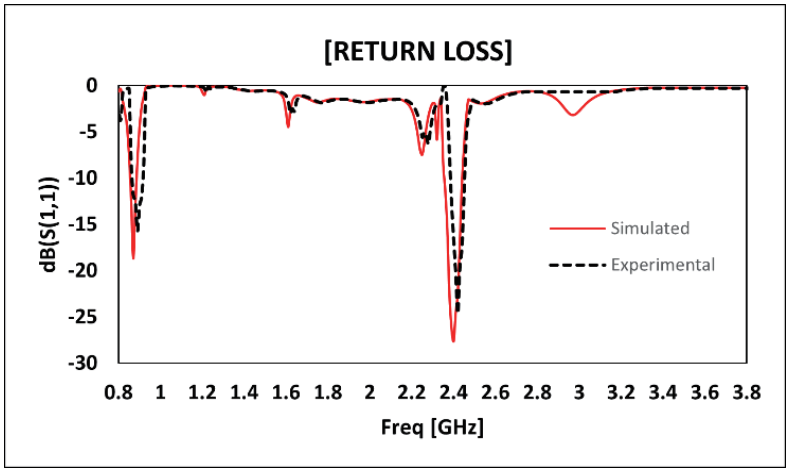

Figure 22. Simulated result v/s measured result analysis.

5. CONCLUSION

A compact circularly polarized polymer-based flexible wearable UHF RFID antenna with an FSS reflector has been designed, analyzed, and fabricated for portable RFID reader which resonates at global UHF band (860–960 MHz) and 2.4 GHz. The periodic frequency selective surface-based reflector is used for gain enhancement, better directivity, reduction of EMI, and stable frequency response throughout the required bandwidth. The proposed RFID antenna is circularly polarized with measured axial ratio bandwidth less than 3 dB. The designed wearable antenna provides better isolation to the electromagnetic interference, avoiding misread of tags, and gain enhancement for longer read range. The flexible frequency selective sheet at the back of the antenna provides better isolation between the body and the patch resulting in lower SAR for on-body wearable applications to meet the safety limit. This RFID antenna can be used efficiently for WBAN applications as a wearable RFID reader for remote sensing and real time monitoring in healthcare.

ACKNOWLEDGMENT

This research work is conducted as a part of Independent Study and Research (ISR) for the award of PhD degree and for the requirement of research project INT/RUS/RFBR/P341 funded by DST, New Delhi.

REFERENCES

1. Paracha, K. N., S. K. Abdul Rahim, P. J. Soh, and M. Khalily, "Wearable antennas: A review of materials, structures, and innovative features for autonomous communication and sensing," *IEEE Access*, Vol. 7, 56694–56712, 2019.
2. Zhao, B., J. Mao, J. Zhao, H. Yang, and Y. Lian, "The role and challenges of body channel communication in wearable flexible electronics," *IEEE Trans. Biomed. Circuits Syst.*, Vol. 14, No. 2, 283–296, 2020.
3. Ahmed, S., S. T. Qureshi, L. Sydänheimo, L. Ukkonen, and T. Björninen, "Comparison of wearable E-textile split ring resonator and slotted patch RFID reader antennas embedded in work gloves," *IEEE Journal of Radio Frequency Identification*, Vol. 3, No. 4, 259–264, 2019.
4. "FCC report and order for Part 15: Acceptance of ultra wideband (UWB) systems from 3.1–10.6 GHz," *FCC*, Washington, DC, USA, 2002.

5. Taylor, P. S. and J. C. Batchelor, "Finger-worn UHF far-field RFID tag antenna," *IEEE Antennas and Wireless Propagation Letters*, Vol. 18, No. 4, 2513–2517, 2019.
6. Parthiban, P., "Fixed UHF RFID reader antenna design for practical applications: A guide for antenna engineers with examples," *IEEE Journal of Radio Frequency Identification*, Vol. 3, No. 3, 191–204, 2019.
7. Kim, J., A. S. Campbell, B. E. de Avila, and J. Wang, "Wearable biosensors for healthcare monitoring," *Nat. Biotechnol.*, Vol. 37, No. 4, 389–406, 2019.
8. Ashyap, A. Y. I., et al., "An overview of electromagnetic band-gap integrated wearable antennas," *IEEE Access*, Vol. 8, 7641–7658, 2020.
9. Tajin, M. A. S. and K. R. Dandekar, "Pattern reconfigurable UHF RFID reader antenna array," *IEEE Access*, Vol. 8, 187365–187372, 2020.
10. Arif, A., M. Zubair, M. Ali, M. U. Khan, and M. Q. Mehmood, "Compact, low-profile fractal antenna for wearable on-body WBAN applications," *IEEE Antennas and Wireless Propagation Letters*, Vol. 18, No. 5, 981–985, 2019.
11. Alqadami, A. S. M., K. S. Bialkowski, A. T. Mobashsher, and A. M. Abbosh, "Wearable electromagnetic head imaging system using flexible wideband antenna array based on polymer technology for brain stroke diagnosis," *IEEE Trans. Biomed. Circuits Syst.*, Vol. 13, No. 1, 124–134, 2019.
12. El Atrash, M., M. A. Abdalla, and H. M. Elhennawy, "A wearable dual-band low profile high gain low SAR antenna FSS-backed for WBAN applications," *IEEE Transactions on Antennas and Propagation*, Vol. 67, No. 3, 6378–6388, 2019.
13. Le, T. T. and T.-Y. Yun, "Miniaturization of a dual-band wearable antenna for WBAN applications," *IEEE Antennas and Wireless Propagation Letters*, Vol. 19, No. 1, 1452–1456, 2020.
14. Zhang, K., G. A. E. Vandenbosch, and S. Yan, "A novel design approach for compact wearable antennas based on metasurfaces," *IEEE Transactions on Biomedical Circuits and Systems*, Vol. 14, No. 4, 918–927, 2020.
15. Gao, G., C. Yang, B. Hu, R. Zhang, and S. Wang, "A wearable PIFA with an all-textile metasurface for 5 GHz WBAN applications," *IEEE Antennas and Wireless Propagation Letters*, Vol. 18, No. 2, 288–292, 2019.
16. Haydhah, S. A., F. Ferrero, L. Lizzi, M. S. Sharawi, and A. Zerguine, "A multifunctional compact pattern reconfigurable antenna with four radiation patterns for sub-GHz IoT applications," *IEEE Open Journal of Antennas and Propagation*, Vol. 2, 613–622, 2021.
17. Wasfy, M. and H. Hammad, "Modelling and design of a large segmented loop antenna with a coplanar parasitic slot loop for NF UHF RFID readers," *IEEE Journal of Radio Frequency Identification*, Vol. 6, 31–40, 2022.
18. Ahmed, G., et al., "Rigorous analysis and evaluation of specific absorption rate (SAR) for mobile multimedia healthcare," *IEEE Access*, Vol. 6, 29602–29610, 2018.
19. Dey, S., M. S. Arefin, and N. C. Karmakar, "Design and experimental analysis of a novel compact and flexible super wide band antenna for 5G," *IEEE Access*, Vol. 9, 46698–46708, 2021.
20. Sharma, S., M. R. Tripathy, and A. K. Sharma, "Low profile and low SAR flexible wearable patch antenna for WBAN," *8th International Conference on Signal Processing and Integrated Networks (SPIN)*, 1119–1124, 2021.
21. Can, S. and A. E. Yılmaz, "Reduction of specific absorption rate with artificial magnetic conductors," *Int. J. RF Microw. Comput. Aided Eng.*, Vol. 26, No. 4, 349–354, 2016.
22. Sharma, S., M. R. Tripathy, and A. K. Sharma, "High gain FSS integrated slotted UHF RFID antenna for WBAN," *Int. J. Syst. Assur. Eng. Manag.*, 2021, https://doi.org/10.1007/s13198-021-01352-z.
23. Sharma, S., M. R. Tripathy, and A. K. Sharma, "Dual-band circularly polarized wearable patch antenna for RFID reader," *IEEE International Conference on RFID Technology and Applications (RFID-TA)*, 195–198, 2021.

24. Liu, X., Y. Liu, and M. M. Tentzeris, "A novel circularly polarized antenna with coin-shaped patches and a ring-shaped strip for worldwide UHF RFID applications," *IEEE Antennas and Wireless Propagation Letters*, Vol. 14, 707–710, 2015.
25. Lai, F.-P., J.-F. Yang, and Y.-S. Chen, "Compact dual-band circularly polarized antenna using double cross dipoles for RFID handheld readers," *IEEE Antennas and Wireless Propagation Letters*, Vol. 19, No. 1, 1429–1433, 2020.
26. Lorenzo, J., A. Lázaro, R. Villarino, and D. Girbau, "Modulated frequency selective surfaces for wearable RFID and sensor applications," *IEEE Transactions on Antennas and Propagation*, Vol. 64, No. 3, 4447–4456, 2016.
27. Saeed, S. M., C. A. Balanis, C. R. Birtcher, A. C. Durgun, and H. N. Shaman, "Wearable flexible reconfigurable antenna integrated with artificial magnetic conductor," *IEEE Antennas and Wireless Propagation Letters*, Vol. 16, 2396–2399, 2017.
28. Lazaro, A., A. Ramos, D. Girbau, and R. Villarino, "A novel UWB RFID tag using active frequency selective surface," *IEEE Trans. Antennas Propag.*, Vol. 61, No. 3, 1155–1165, Mar. 2013.
29. Sharma, S., M. R. Tripathy, and A. K. Sharma, "FSS supported longer read range passive UHF RFID reader antenna," *IEEE International Conference on RFID Technology and Applications (RFID-TA)*, 207–210, 2021.
30. Pozar, D. M. and D. H. Schaubert, *Microstrip Antennas: The Design and Analysis of Microstrip Antennas and Arrays*, 4th Edition, John Wiley and Sons, 2012.
31. Munk, B. A., *Frequency Selective Surfaces: Theory and Design*, Wiley, New York, 2000.
32. Ziolkowski, R. W., "Design, fabrication, and testing of double negative metamaterials," *IEEE Transactions on Antennas and Propagation*, Vol. 51, No. 7, 1516–1529, 2003.
33. Can, S. and A. E. Yılmaz, "Reduction of specific absorption rate with artificial magnetic conductors," *Int. J. RF Microw. Comput. Aided Eng.*, Vol. 26, No. 4, 349–354, 2016.
34. Fakhte, R. and I. Aryanian, "Compact fabry-perot antenna with wide 3 dB axial ratio bandwidth based on FSS and AMC structures," *IEEE Antennas and Wireless Propagation Letters*, Vol. 19, No. 1, 1326–1330, 2020.
35. Sarkar, S. and B. Gupta, "A dual-band circularly polarized antenna with a dual-band AMC reflector for RFID readers," *IEEE Antennas and Wireless Propagation Letters*, Vol. 19, No. 5, 796–800, 2020.
36. Ashyap, A. Y. I., et al., "Highly efficient wearable CPW antenna enabled by EBG-FSS structure for medical body area network applications," *IEEE Access*, Vol. 6, 77529–77541, 2018.
37. Wang, M., et al., "Investigation of SAR reduction using flexible antenna with metamaterial structure in wireless body area network," *IEEE Trans. Antennas Propag.*, Vol. 66, No. 6, 3076–3086, 2018.
38. Lai, F.-P., J.-F. Yang, and Y.-S. Chen, "Compact dual-band circularly polarized antenna using double cross dipoles for RFID handheld readers," *IEEE Antennas and Wireless Propagation Letters*, Vol. 19, No. 1, 1429–1433, 2020.
39. Singh, R. K., A. Michel, P. Nepa, A. Salvatore, M. Terraroli, and P. Perego, "Compact and wearable yagi-like textile antennas for near-field UHF-RFID readers," *IEEE Transactions on Antennas and Propagation*, Vol. 69, No. 3, 1324–1333, 2021.
40. Ahmed, S., D. Le, L. Sydänheimo, L. Ukkonen, and T. Björninen, "Wearable metasurface-enabled quasi-yagi antenna for UHF RFID reader with end-fire radiation along the forearm," *IEEE Access*, Vol. 9, 77229–77238, 2021.